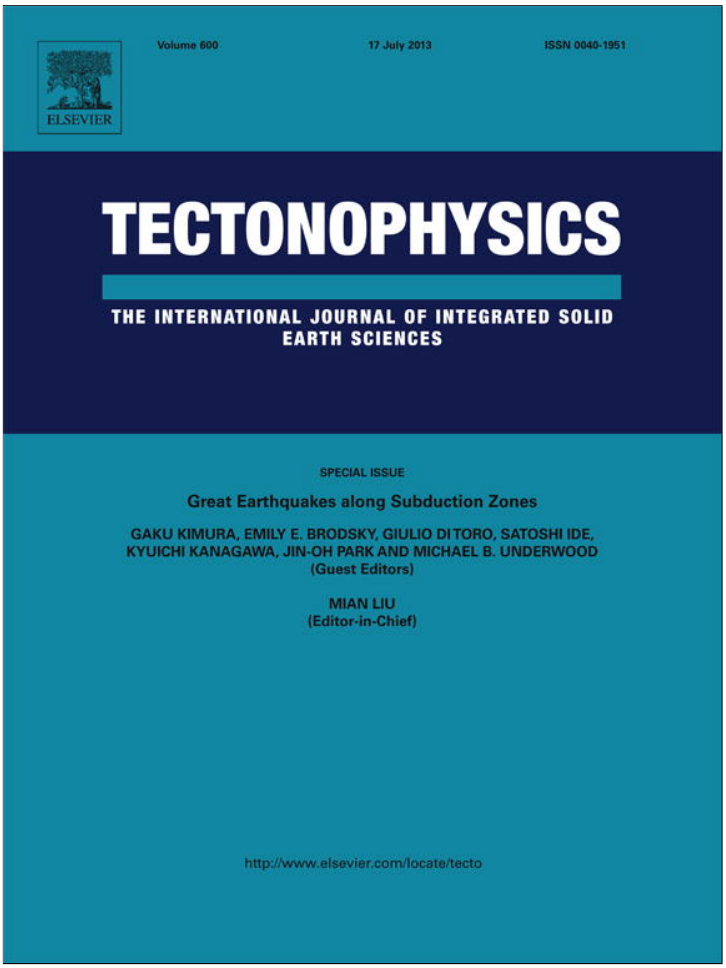

Tectonophysics 600 (2013) 196–204

Contents lists available at SciVerse ScienceDirect

Tectonophysics

journal homepage: www.elsevier.com/locate/tecto

Earthquake cycle simulation with a revised rate- and state-dependent friction law

Nobuki Kame *, Satoshi Fujita, Masao Nakatani, Tetsuya Kusakabe

Earthquake Research Institute, the University of Tokyo, 1-1-1 Yayoi, Bunkyo-ku, Tokyo 113-0032, Japan

ARTICLE INFO

Article history:
Received 1 June 2012
Received in revised form 8 November 2012
Accepted 23 November 2012
Available online 11 December 2012

Keywords:
Rate- and state-dependent friction
Earthquake cycle
Earthquake precursor
Critical stiffness

ABSTRACT

Rate- and state-dependent friction law (RSF) has been recently revised by Nagata et al. (2012); the value of direct effect parameter has been revised to be five times greater, and a newly noticed weakening effect by shear stress has been incorporated. Using this revised RSF that seems to have eventually resolved all the known discrepancies from laboratory observations, we re-investigated the mechanics of stick-slip cycles. Using a spring-slider model, we analyzed the long-term stability and derived the critical stiffness. We then simulated stick-slip cycles with both the original and revised RSFs. Two significant differences have been recognized. 1) With the revised RSF, the state turns to decrease as early as at one-third of the recurrence interval, when the fault is still firmly locked. This contrasts to the result with the original RSF where the turning point comes much later as the slip becomes fast enough for the slip-weakening term to beat the healing term. 2) State reduction in the short-term preslip period, defined as the period since the slip velocity exceeds the load-point velocity, is three times larger for the revised RSF. The former is a direct manifestation of the stress-weakening effect, and the latter is attributed to the larger slip-weakening rate in the revised RSF. On the other hand, stress or slip velocity history did not differ very much. It is suggested that monitoring for precursory weakening of the interface, as has been successfully done by an acoustic method in the laboratory, is advantageous over the monitoring for preslip by geodetic methods, especially when we consider the revised RSF.

1. Introduction

The rate- and state-dependent friction law (RSF) was first introduced by Dieterich (1979) on the basis of laboratory rock friction experiments and has been extensively used in fault mechanics. Because RSF covers a wide range of slip velocities, many studies have adopted it to simulate seismic cycles. RSF successfully explained earthquake cycles from quasi-static sliding in nucleation to high-speed sliding in dynamic rupture (e.g., Lapusta et al., 2000). It must be emphasized that RSF can explain a variety of slip behaviors such as postseismic afterslip (e.g., Marone et al., 1991), earthquake nucleation (e.g., Dieterich, 1992) and aftershock activity (e.g., Dieterich, 1994).

The fact that it is based on laboratory measurements is the main justification for the use of RSF for fault mechanics modeling. However, it has been long recognized that RSF has clear shortcomings in reproducing laboratory results (e.g. Beeler et al., 1994; Kato and Tullis, 2001; Marone, 1995). Several different formulae have been proposed to overcome the problem, but none of them were free from some drawbacks that contradict some reproducible aspects of laboratory results (e.g., Nakatani, 2001) until Nagata et al. (2012) came up with a fairly drastic revision. Furthermore, different formulae sometimes lead to important differences in the modeled behavior. For example, numerical simulations of seismic cycles vary significantly depending on the formula adopted (e.g., Rice and Ben-Zion, 1996). Qualitative patterns of earthquake nucleation also depend strongly on the adopted formula (Ampuero and Rubin, 2008). Very recently the revised RSF of Nagata et al. (2012) was adopted in simulation of aftershock triggering and qualitative differences from the previously proposed formulae were found (Kame et al., 2012). In the present paper, we examine the behavior of earthquake cycles simulated with the revised RSF that seems to have no flaws in describing laboratory data. We limit our simulations to the single degree-of-freedom spring-slider model and examine the difference by comparison with simulations with the 'slowness' version of traditional RSF formula, which is popular in fault mechanics modeling and also is the direct predecessor of the Nagata et al.'s (2012) version.

2. Background: Existing and revised RSFs

Following Nagata et al. (2012), we briefly summarize the existing and revised RSFs. RSF has been proposed as an empirical friction law (Dieterich, 1979; Ruina, 1983). RSF consists of two equations bearing logically separate roles. First is the constitutive law, which describes the relationship between applied shear stress and slip velocity as

$$V = V_* exp\left[\frac{\tau - \Phi}{a\sigma}\right], \quad \text{or} \quad \tau = \Phi + a\sigma \ln\left(\frac{V}{V_*}\right), \tag{1}$$

* Corresponding author. Tel.: +81 3 5841 5694; fax: +81 3 5802 3391.
E-mail address: kame@eri.u-tokyo.ac.jp (N. Kame).

0040-1951/$ – see front matter © 2012 Elsevier B.V. All rights reserved.
http://dx.doi.org/10.1016/j.tecto.2012.11.029

where τ and σ are the shear and normal stresses, respectively, V is the slip velocity, V_* is an arbitrarily chosen reference velocity, a is a nondimensional positive parameter called the direct effect coefficient, and Φ is the state variable specifying the internal physical state of the interface, which in many cases, may reflect the real contact area (Dieterich and Kilgore, 1996). The parameter a plays a central role in the constitutive law (Nakatani, 2001) and the physical mechanism behind it has been attributed to thermally activated creep (Heslot et al., 1994; Nakatani, 2001). In macroscopic view, Φ can be considered as an extension of classical frictional strength because Φ is the shear stress required to move the interface at a reference velocity V_* (Nakatani, 2001). Throughout this paper we call Φ either state or strength, depending on the context. The second equation is the evolution law, which phenomenologically describes variations of the state Φ. One popular model of the evolution law, called the 'slowness law' or the Dieterich law (e.g., Beeler et al., 1994), is written as

$$\frac{d\Phi}{dt} = \frac{b\sigma}{L} V_* exp\left[-\frac{\Phi-\Phi_*}{b\sigma}\right] - \frac{b\sigma}{L} V, \tag{2}$$

where L is a characteristic length dimension and Φ_* is a reference state. The first term of Eq. (2) represents logarithmic time-dependent healing, while the second term represents linear slip-weakening with a constant weakening rate b/L per unit slip (Nakatani, 2001). The Dieterich law explains time-dependent healing very well as observed, but has trouble in reproducing an exponential change of friction over a fixed slip distance as repeatedly observed in experiments (e.g., Nakatani, 2001; Ruina, 1983; Weeks, 1993). Related to this shortcoming is a well-known difficulty in reproducing the observed symmetric evolutions subsequent to stepwise velocity jumps of opposite signs (e.g., Kato and Tullis, 2001; Marone, 1995). Physical mechanism behind the logarithmic time-dependent healing is thought to be an increase of the real contact area (e.g., Scholz and Engelder, 1976) and has been quantitatively modeled by considering plastic squashing of asperity contacts driven by normal stress (Brechet and Estrin, 1994; Nakatani and Scholz, 2004b).

Another popular evolution law model, called the 'slip law' or the Ruina law (e.g., Beeler et al., 1994), is good at reproducing the exponential slip-dependent change of friction, but it wrongly denies the truly time-dependent healing, contradicting experiments (e.g. Beeler et al., 1994; Nakatani and Mochizuki, 1996). Since this is a very clear and fundamental shortcoming in terms of physics, we do not discuss the Ruina law in this paper.

Recently Nagata et al. (2012) proposed a revised RSF, using new rigorous methods of experimental data analysis. Firstly, the direct effect coefficient a was constrained to be 0.05, about five times larger than previously believed. The difference came from their new method to constrain the direct effect without using any evolution laws, contrasting to conventional methods where the state change coming from imperfection of real-world 'step' tests was inferred by assuming some evolution law. The large a immediately led to similarly large $b \sim 0.05$ because $(b-a) \sim 0$ was directly and reliably constrained from velocity dependence of steady-state friction. Secondly, they found a previously unknown weakening effect caused by a shear stress increase, using another new method called misprediction analysis; a systematic deviation, throughout different types of experiments, was found between the actual Φ $(=\tau - a\sigma ln(V/V_*))$ calculated from the measured (V,τ,σ) with the correct a-value and the Φ predicted by the slowness version of evolution law (Eq. (2)) with the measured slip history substituted. The revealed misprediction in $\dot{\Phi}$ showed a strong linear negative dependence on $\dot{\tau}$. They accordingly proposed a revised evolution law (the Nagata law) as

$$\frac{d\Phi}{dt} = \frac{b\sigma}{L} V^* exp\left[-\frac{\Phi-\Phi_*}{b\sigma}\right] - \frac{b\sigma}{L} V - c\frac{d\tau}{dt}, \tag{3}$$

where c is the coefficient of the stress weakening and was determined to be approximately 2.0 from the above misprediction analysis. They speculated that the stress-weakening effect involved elastic tilting of the asperities that would tear some junction bonds.

By using the revised RSF, Nagata et al. (2012) could reproduce both hold-slide and velocity-step tests correctly as shown in Fig. 1. It must be noted that different types of experiments were fitted well with the same values of frictional parameters. This had not, in fact, been achieved with conventional RSFs.

A further very important achievement is that the Nagata law can reproduce the evolution of the state correctly as well as the shear stress. Studies before Nagata et al. (2012) only cared the match of shear stress history, not checking if the state $(\Phi = \tau - a\sigma ln(V/V_*))$ was reproduced correctly. However, noting that the constitutive law Eq. (1) for a given a leaves only two of the three (Φ, V, τ) variables independent of each other, severe misprediction of the state is effectively demonstrated by the severe misprediction of slip velocity as pointed out by Nakatani (2001).

In addition, note that the amplitude of P-wave transmitted across the frictional interface tracks Φ very well as shown in Fig. 1. This implies that the internal state variable Φ is indeed a physical reality, that can be observed directly (e.g., Dieterich and Kilgore, 1996; Nagata et al., 2008; Pyrak-Nolte et al., 1990).

The best-fit simulation results with the original (Dieterich) and the revised (Nagata) RSFs for the velocity-step tests of Fig. 1 are plotted in Fig. 2a. Here the Dieterich RSF means Eq. (1) with a traditional a-value and Eq. (2), while the Nagata RSF means Eq. (1) with the revised a-value and Eq. (3). Reproduction of shear stress was fine with either RSF because parameters were adjusted to fit the shear stress data. However, the original RSF mispredicted the slip velocity, which actually means misprediction of the state as mentioned earlier. In cycle simulations of the present paper, we will pay attention to the history of both slip velocity and state variable, while earlier studies tended to focus on slip velocity only.

3. Choice of frictional parameter sets

3.1. Parameter sets obtained from the actual velocity-step tests of Nagata et al. (2012)

In earlier studies exploring the effects of different RSF formulae (e.g., Gu et al., 1984; Kato and Tullis, 2003; Rubin and Ampuero, 2005), the parameter (a, b, L) values to fit the same experimental data did not depend much on the specific formula. However, the revision by Nagata et al. (2012) involves a drastic change in parameter values from the original Dieterich RSF. Therefore, it is not appropriate to compare predictions by both laws with the same values of the parameters. Instead, the parameter sets that fit the same experimental data with each formula must be regarded as counterparts. We use the experimental data of Nagata et al. (2012) as a reference data set (called data N hereafter) and obtain different sets of parameters by the fitting of this same data with each formula. Further, noticing that setting $c=0$ in Nagata law leads to the Dieterich law, we see that the parameter c tunes 'Nagataness'. Nagata et al. (2012) found $c=2.0$ to be the optimum, but we prepare three sets of parameter values by fitting the same experimental data N with c fixed to 0, 2, or 4. The set with $c=0$ (denoted N-0) is the pure Dieterich law, $c=2$ (set N-2) represents the appropriately Nagatish set, and $c=4$ (set N-4) represents an overly Nagatish set. Parameter values for these sets are shown in Table 1. Fig. 2a shows stress histories simulated with each of the three parameter sets. In just reproducing the stress-vs-slip curve, all the three sets did a fair job.

3.2. Parameter sets obtained from two sets of supplementary data

In Nagata et al. (2012), data N were the only reference data for which frictional parameters were determined. In order to check the

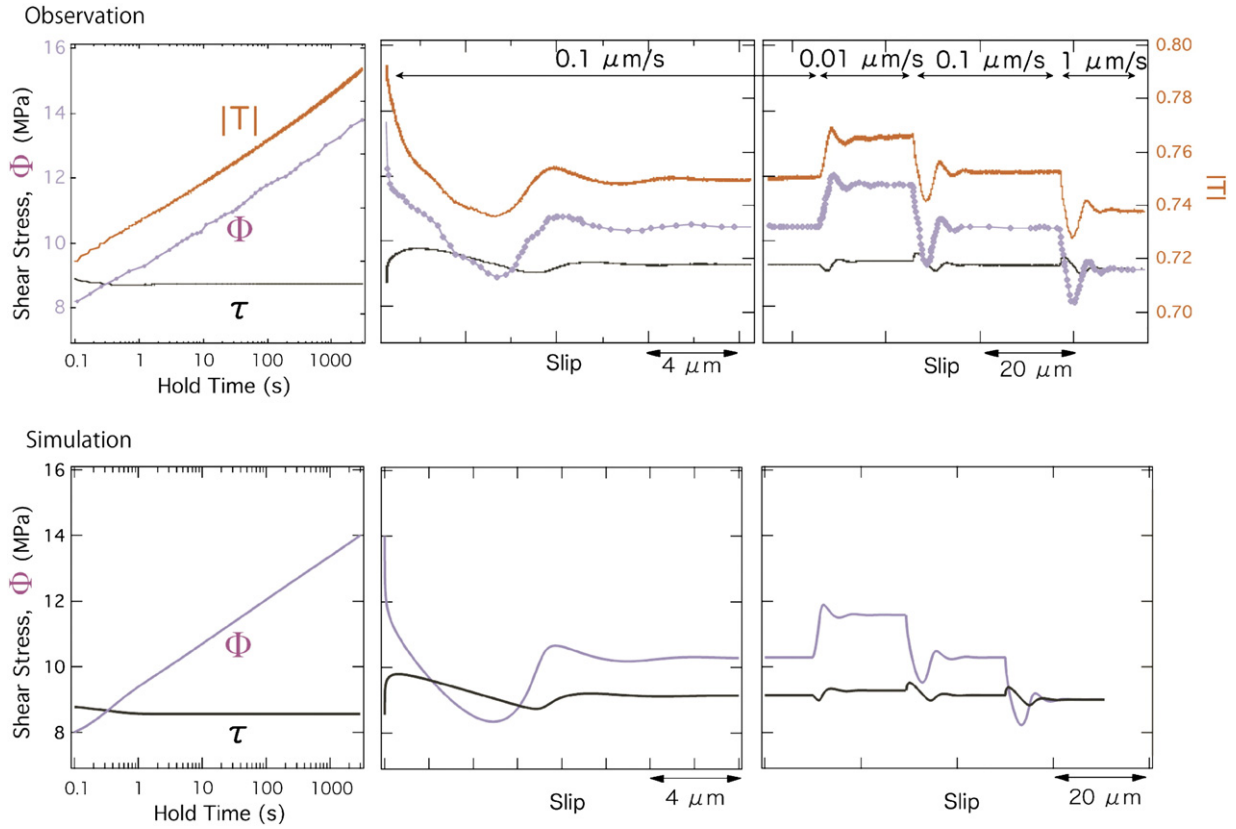

Fig. 1. Comparison of Φ (state, or strength) and τ (shear stress) between observations and simulations for various types of experiments, such as a hold under a constant shear stress (left column), reloading after the hold (middle column), steady-state sliding at different velocities (right column) from Fig. 16 of Nagata et al. (2012). |T| is the acoustic transmissivity measured by the amplitude of P wave traveled across the interface. The simulations are based on the revised RSF with the parameter set N-2 in Table 1.

robustness of tendencies of earthquake cycles depending on different RSF versions, we prepare two more sets of parameter values that fit two more sets of supplementary reference data, which were artificially created to mimic experimental results on surfaces with different frictional properties.

Data A represent (imaginary) test results expected of a frictional interface having a twice greater direct effect a and the same $(b\text{-}a)$ as N-2. Data B represent another imaginary case with the same direct effect a and a three times greater $(b\text{-}a)$ value than N-2. As $(a\text{-}b)$ represents the velocity dependence of steady-state friction, a more positive value of $(b\text{-}a)$ means stronger velocity weakening. These two sets of supplementary data were generated by simulating velocity-step tests by using the Nagata law assuming $c=2.0$ (optimally Nagatish) and $L=0.33\mu$m. Namely we assume $(a, b, c, L)=(0.102, 0.1075, 2.0, 0.33\ \mu\text{m})$ for data A and $(a, b, c, L)=(0.051, 0.069, 2.0, 0.33\ \mu\text{m})$ for data B, which are denoted as A-2 and B-2, respectively.

We then determined frictional parameters that gave best fitting to data A and data B, with various degrees of Nagataness presumed by setting $c=0.0$ or 4.0. Resulting friction parameter sets are denoted as A-0, A-4, B-0 and B-4, respectively (Table 1). Fig. 2b and c show simulated velocity-step tests with these six parameter sets. In summary, Data A, B and N represent physical variation of frictional properties dependent on the experimental conditions and the rock type, while -0, -2 and -4 represent the trim of the friction law to describe the data.

4. Stability analysis of a single-degree-of-freedom system

In this section, we investigate the stability of frictional sliding with the Nagata RSF. We derive the critical stiffness k_c, which needs to be considered in cycle simulations in Section 5.

We consider a simple spring-slider model (Fig. 3). A rigid massless slider with displacement δ is in frictional contact under a normal stress σ. The load point is connected to the slider by a spring of stiffness k which transmits the shear stress τ from the load point with displacement u. We assume a constant load-point velocity $\dot{u}=V_0$, where dot denotes time differentiation. For simplicity, we assume a constant normal stress σ throughout the present paper. From the force balance between the friction and the spring shear stress, we obtain

$$\dot{\tau}=k(V_0-V), \tag{4}$$

where $V\left(=\dot{\delta}\right)$ is the slider velocity.

The following analysis is identical to Ruina (1983) except the additional stress-weakening term $-c\cdot\dot{\tau}$ in Eq. (3). We examine the system's long-term stability tendency by looking for solutions near the steady-state solution at the slip velocity $V=V_0$, the stress τ_0, the state Φ_0 and $\dot{\Phi}=0$. Linearizing the friction τ in Eq. (1) and the state Φ in Eq. (3) near this solution, we obtain

$$\tau'=\Phi'+a\sigma\frac{V'}{V_0}, \tag{5}$$

$$\dot{\Phi}'=\frac{V_0}{L}\Phi'-\frac{b\sigma}{L}V'-c\dot{\tau}', \tag{6}$$

where $\tau'=\tau-\tau_0$, $V'=V-V_0$ and $\Phi'=\Phi-\Phi_0$. On the other hand, linearizing Eq. (4) gives

$$\dot{\tau}'=-kV'. \tag{7}$$

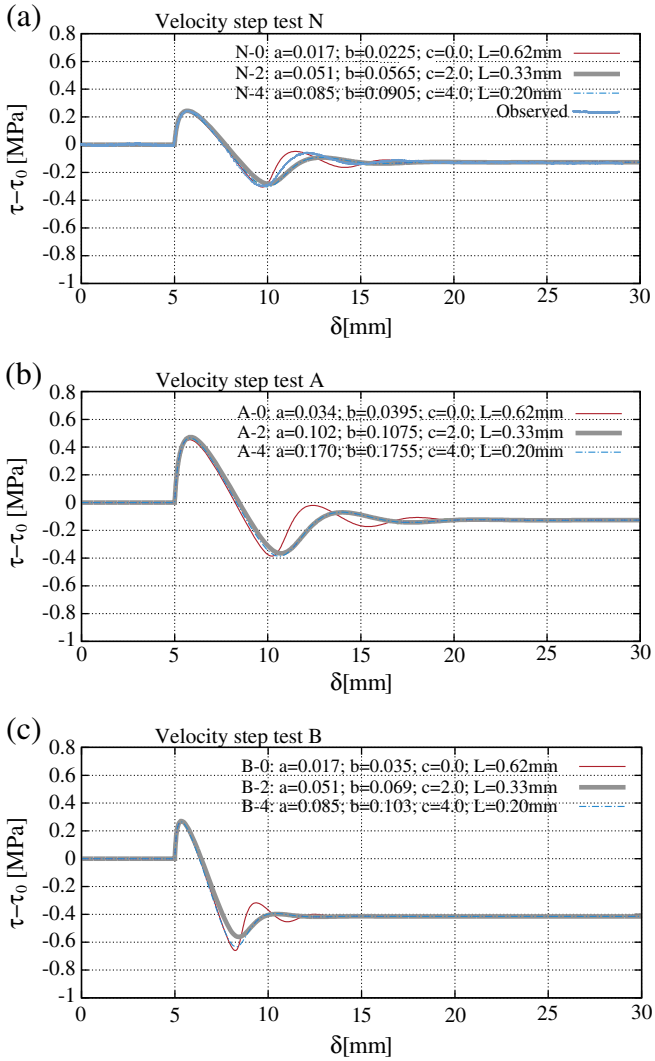

Fig. 2. Stress histories simulated for a positive velocity step test (from 0.01 μm/s to 0.1 μm/s) with each of the nine parameter sets in Table 1. Top panel for N-0,-2,4 and the observed stress history being fit; middle panel for A-0,-2,-4 and bottom panel for B-0,-2,4. '-0,-2,4' represents c coefficient of stress-weakening effect.'-0' is the Dieterich RSF, '-2' is the Nagata RSF and '-4' is overly stress-weakening. In all plots, $k=0.2$ MPa/μm and $\sigma=10$MPa as employed in Nagata et al. (2012).

By eliminating V' and Φ' from Eqs. (5), (6) and (7), we obtain a differential equation with respect to τ' as

$$\left(\frac{a\sigma}{kV_0}\right)\ddot{\tau}' + \left[(1+c)-\frac{\sigma}{kL}(b-a)\right]\dot{\tau}' + \frac{V_0}{L}\tau' = 0. \tag{8}$$

Table 1
RSF parameters (a, b, c, L) and simulation parameters (L^{sim}, k^{sim}/k_c, v^{sim}).

RSF#	a	b	c	L[μm]	L^{sim}[m]	k^{sim}/k_c	v^{sim}[m/s/MPa]
N-0	0.017	0.0225	0.0	0.62	0.062	0.57	1.09×10^{-3}
N-2	0.051	0.0565	2.0	0.33	0.033	0.90	8.8×10^{-5}
N-4	0.085	0.0905	4.0	0.20	0.020	0.91	3.0×10^{-4}
A-0	0.034	0.0395	0.0	0.62	0.062	0.57	4.0×10^{-1}
A-2	0.102	0.1075	2.0	0.33	0.033	0.90	3.3×10^{-1}
A-4	0.170	0.1755	4.0	0.20	0.020	0.91	5.0×10^{-1}
B-0	0.017	0.035	0.0	0.62	0.062	0.17	1.8×10^{6}
B-2	0.051	0.069	2.0	0.33	0.033	0.27	2.3×10^{5}
B-4	0.085	0.103	4.0	0.20	0.020	0.28	2.0×10^{5}

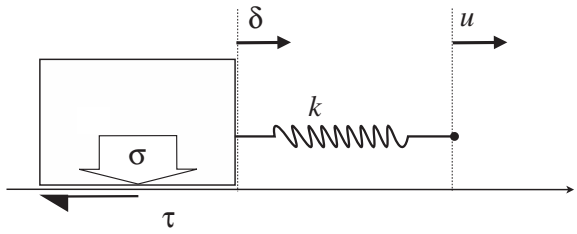

Fig. 3. A simple spring-slider model. A rigid massless slider is pulled by a load point through a spring of stiffness k. u, δ, τ and σ are the displacement of the load point, the displacement of the slider, the frictional shear stress, and the normal stress acting on the slider, respectively.

Then we assume that the solution τ' has a form,

$$\tau' = Ae^{st}, \tag{9}$$

where A is a real constant and s is a complex constant to be determined. By substituting Eq. (9) into Eq. (8), we derive a quadratic equation and solutions for s. If $Re[s]>0$ then τ' grows to infinity, and if $Re[s]<0$ then τ' converges to zero. $Re[s]=0$ thus is the critical condition for the stability of the steady-state sliding, and it leads to the following critical stiffness for the revised RSF,

$$k_c^{rev} = \frac{(b-a)\sigma}{(1+c)L}. \tag{10}$$

This is an extension of the Ruina (1983)'s result of $k_c^{orig}=(b-a)\sigma/L$ for the Dieterich RSF. Indeed, k_c^{rev} coincides with k_c^{orig} when $c=0$.

We below verify the critical stiffness in Eq. (10) numerically in the spring-slider model with the following stiffnesses $k/k_c=10, 2, 1, 0.5$, and 0.2. Theoretically expected behavior in response to a given disturbance is calming down to steady-state sliding for supercritical cases of $k/k_c>1$ and divergence toward stick-slip motion for subcritical cases $k/k_c<1$ (Ruina, 1983). We use the frictional parameter set N-2 in Table 1 with a normal stress $\sigma=10$ MPa and started with the steady-state sliding at $V=\dot{\delta}=0.7\mu$m/s. When the slider displacement reached $\delta=5$ μm, the load-point velocity was suddenly changed to 1 μm/s, and the subsequent slip history was numerically simulated. Fig. 4 shows the results. The results perfectly accorded with the theory, including the sustained oscillation for $k/k_c=1$.

Here we briefly discuss the values of traditional k_c^{orig} and the revised k_c^{rev}. Based on data N, i.e., the actual experimental data of Nagata et al. (2012), N-0 and N-2 with $\sigma=10$ MPa leads to $k_c^{orig}=0.080$ MPa/μm and $k_c^{rev}=0.055$ MPa/μm, respectively, meaning that faults (,which obeys the Nagata RSF in fact,) are somewhat more stable than previously inferred from the Dieterich description of laboratory data. Note that the actual machine stiffness of Nagata et al. (2012) was about $k=0.20$ MPa/μm, stiff enough to conduct frictional experiments under a perfectly stable condition for both k_c^{orig} and k_c^{rev}.

In the following section, we simulate seismic cycles assuming a k lower than both k_c^{orig} and k_c^{rev} because our interest is unstable stick-slip motion of earthquake faults.

5. Simulation of seismic cycles

We simulate regular stick-slip cycles obeying the Dieterich and Nagata RSFs in order to elucidate differences made by the Nagata RSF. We emphasize that the Nagata RSF is so far the only friction law that properly represents the two fundamental processes of seismic cycles, i.e., slip weakening and time-dependent healing, added to the fundamental advantage shared by all versions of RSF, i.e., the finite slip velocity as a continuous function of the applied stress (i.e., direct effect, Nakatani, 2001; Rice et al., 2001) even at stresses lower than the nominal frictional strength.

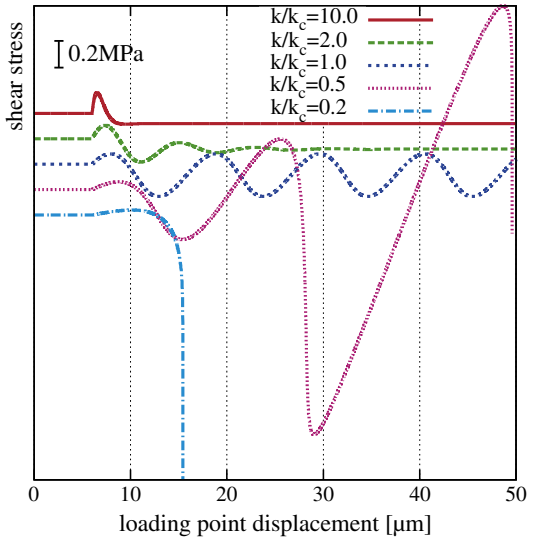

Fig. 4. Frictional shear stress τ versus load-point displacement δ in the spring-slider model of Fig. 3. After steady-state sliding at 0.7 μm/s, the load-point velocity is suddenly increased to 1.0 μm/s. Subsequent motion for various k are shown, as calculated with RSF parameter set N-2 in Table 1.

5.1. Spring-slider model with radiation damping approximation

In the present paper, earthquake cycle simulation is performed for a massless spring-slider system controlled by RSF. Complete negligence of inertial effects, however, leads to situations in which the slip velocity increases without bound (Fig. 4), making simulations of repeated stick-slip cycles impossible. Following many earlier authors, we get around the problem by use of so-called radiation damping approximation rather than explicit consideration of inertia as $m \cdot dV/dt$. The equation of motion becomes

$$k(V_0 t - \delta) - \tau = \nu \dot{\delta}, \tag{11}$$

where $\nu = \mu/2\beta$, μ is the rigidity, and β is the shear wave velocity (Rice, 1993). The damping term is introduced to represent energy dissipation due to seismic wave radiation in a continuum. $m \cdot dV/dt$ is correct for a lumped mass, but, not for continuum and may predict excessive dynamic overshoot because of no wave radiation.

The damped equation of motion Eq. (11) coupled with the RSF (Eqs. (1) and (3)) is solved using a Runge–Kutta method (Press et al., 1992). We tried with the nine sets of friction parameter sets listed in Table 1. We assume the load-point velocity $V_0 = 4.5$ cm/year, the normal stress $\sigma = 100$ MPa, and the spring stiffness $k^{sim} = 5.0$ MPa/m throughout our simulations. The characteristic length L^{sim} in the simulations is assumed to be 10^5 times larger than the laboratory value because L is scale dependent, affected by, for example, the thickness of the gouge layer (e.g., Chambon et al., 2006; Marone and Kilgore, 1993). The damping coefficient ν^{sim} is adjusted so that the earthquake recurrence interval becomes $T_r = 100$ years, which effectively sets the static stress drop common to simulations with different parameter sets. The nine sets of parameters are listed in Table 1. It must be noted that our current choice of ν^{sim} does not represent physical characteristics (μ and β) of the surrounding elastic medium, where ν^{sim} varies by 10 orders of magnitude in Table 1. Accordingly, results of the dynamic parts of our simulation should not be used to derive any conclusions. However, quasi-static behavior, the target of this paper, is not affected by ν^{sim}.

At the beginning of the simulation, the loading velocity and the sliding velocity are 3.0 cm/year and the initial shear stress is the steady-state value. The loading velocity is then suddenly increased to 4.5 cm/year ($= V_0 = 1.4 \times 10^{-9}$ m/s) in order to begin stick-slip cycles. In all simulations shown in the present paper, the system settled to cyclic stick-slip motion with a regular interval and amplitude, after a transient period over several stick-slip cycles with varying interval and stress drop. We discuss results from regular stick-slip parts.

5.2. Results

5.2.1. The Dieterich RSF and the Nagata RSF

We first compare simulation results with the Dieterich RSF (N-0) and the Nagata RSF (N-2) based on data N. Fig. 5 shows the simulated histories of the slider displacement δ, the log-velocity $log(V/V_0)$, the shear stress $\tau - \tau_0$ and the state $\Phi - \Phi_0$, where τ_0 and Φ_0 are the steady-state value for V_0. The origin of time $t = 0$ is set to one of dynamic events, at the moment of peak velocity. Seismic slip is approximately 4.5 m, equal to the slip deficit ($V_0 T_r$) expected from the loading velocity and the recurrence interval. Associated stress drop ($= kV_0 T_r$) is 22.5 MPa.

The histories of δ, V and τ with the Dieterich RSF (Fig. 5a) and the Nagata RSF (Fig. 5b) show similar general tendencies. The slider is almost locked for most of the cycle, where $V \ll V_0$, but gradually increases as the shear stress increases. In either case, V exceeds V_0 at $t = -2 \sim -1$ year, by which we define, for convenience sake, the transition from the interseismic to preslip period. The acceleration finally leads to the fast seismic slip, that is, the earthquake occurrence. Here fast slip is arbitrarily defined by a critical velocity $V_c = 10^6 V_0 (= 1.4$ mm/s), which marks the end of preslip period for convenience sake.

On the other hand, state histories show significant differences between the results with the two RSFs. The state in the Dieterich-RSF case keeps increasing for the first 87 years of the cycle and then turns to decrease at $t_{int} = -13$ year, due to the elevated slip velocity that makes action of slip weakening exceed that of healing. Here t_{int} denotes the onset time of strength reduction in the interseismic period. In contrast, in the Nagata-RSF case, the state increases only for the first 33 years, that is, $t_{int} = -67$ year. This very early start of state reduction is a direct manifestation of the newly introduced stress-weakening effect in the Nagata law (Eq. (3)). The equation contains three terms. The first, time-healing term is always positive and hence never causes a state reduction. The second is the negative, slip-weakening term, but this is negligible compared to the healing term at this early stage of cycle, where stress is still much lower than strength Φ, resulting in the slip velocity still negligible. In contrast, the shear stress keeps increasing at a constant loading rate from early on and hence the third term $-c \cdot \dot{\tau}$ takes a significantly negative and approximately constant value throughout the well-locked period of the cycle. Hence, the stress-weakening term can exceed the healing term since a fairly early stage of the cycle as soon as the healing slows down logarithmically due to the increased (healed) state.

Next, we examine behaviors in the preslip stage in detail. Slip velocity V, stress τ and state Φ just for two years prior to instability are shown in Fig. 6, and the characteristic quantities Δt_{pre}, $\Delta \tau_{pre}$, and $\Delta \Phi_{pre}$, are listed in Table 2. As mentioned earlier, preslip period here refers to the period during which slip velocity quasi-statically accelerates from V_0 to $10^6 V_0$. The preslip durations Δt_{pre} for Dieterich RSF and Nagata RSF are similar, being 1.2 years and 2.0 years, respectively. The stress drops $\Delta \tau_{pre}$ during the preslip period are also similar, at 3.6 MPa and 4.9 MPa. In contrast, the state (or, strength) drop $\Delta \Phi_{pre}$ is significantly different: 28 MPa for Dieterich and 76 MPa for Nagata. The larger strength drop with the Nagata RSF is attributed to the larger rate of slip-weakening b/L in the Nagata evolution law (Eq. (3)). The first healing term is always positive again, and the third stress-weakening term $-c \cdot \dot{\tau}$ turns positive in the preslip period during which stress is slightly decreasing. Only the second slip-weakening term can reduce the strength. Slip-weakening rate $b\sigma/L$ is 36.3 MPa/m in the Dieterich RSF (N-0 in Table 1) and $b\sigma/L = 171$ MPa/m in the Nagata RSF (N-2 in Table 1). The rate in the Nagata RSF is about five

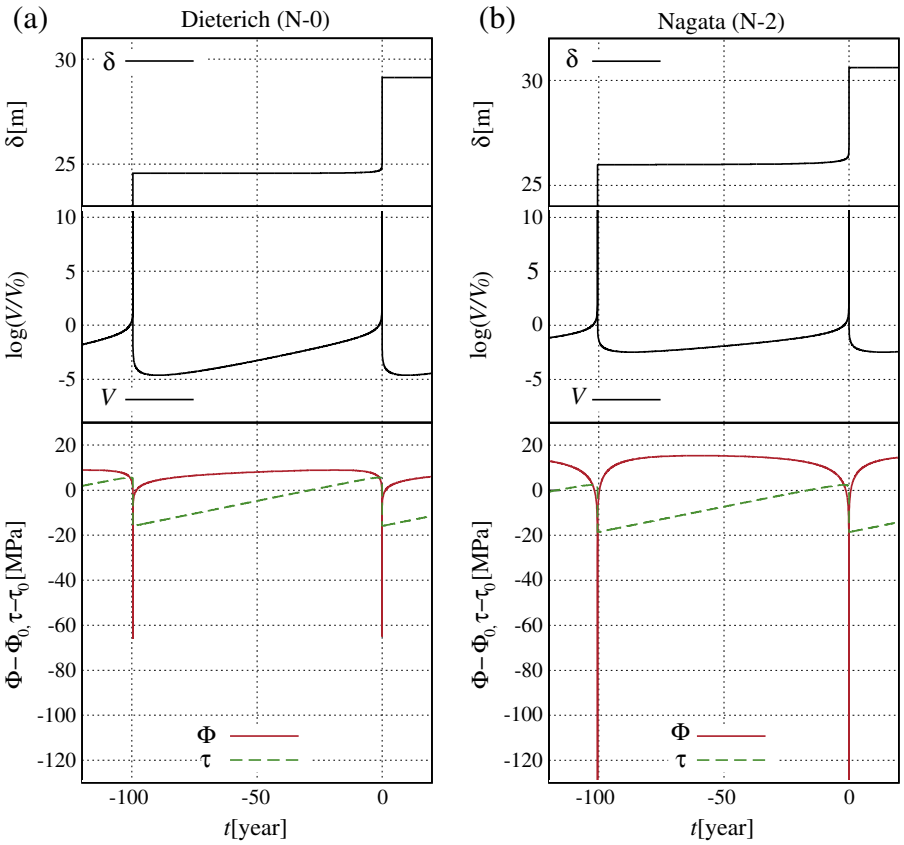

Fig. 5. Simulated histories of the slider displacement δ (top), the slider velocity normalized by the load point velocity V/V_0 (middle), the state Φ and the shear stress τ (bottom) for the Dieterich RSF (left column) and the Nagata RSF (right column), where Φ_0 and τ_0 are steady-state values for V_0.

times larger than that in the Dieterich RSF, causing the larger strength drop during its preslip phase.

To further check the effects of the Nagataness of the friction law, another simulation was done with the frictional parameter set N-4. It is based on the same data N but is an overly Nagatish description with a stronger stress-weakening effect with $c=4.0$. The result (Table 2) showed a further earlier state decrease beginning at $t_{int}=-70$ year. Slip-weakening rate in the evolution law was $b\sigma/L=452$ MPa/m and

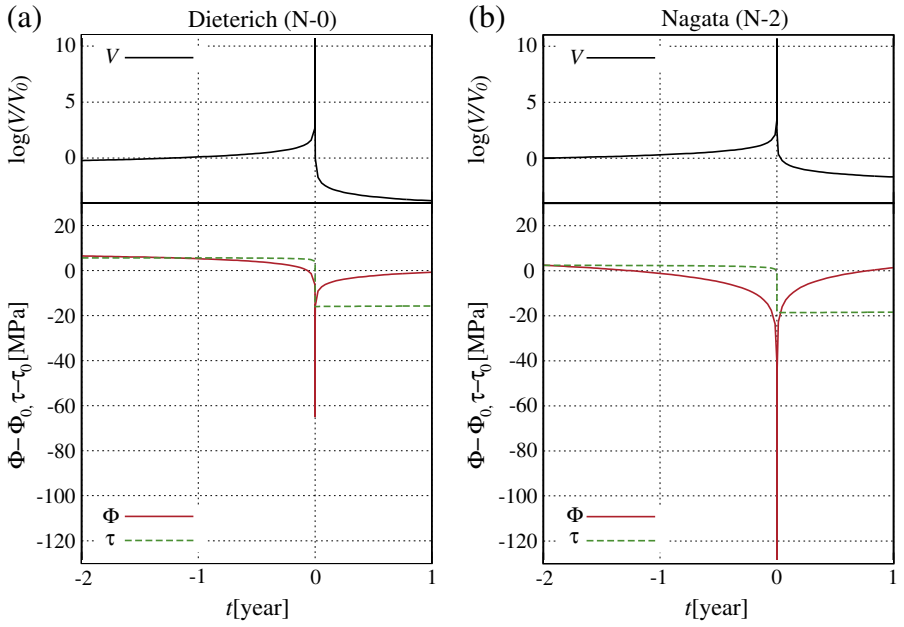

Fig. 6. Simulated histories for two years prior to instability at $t=0$. The slider velocity normalized by the load point velocity V/V_0 (top), the state Φ, and the shear stress τ (bottom) for the Dieterich RSF (left column) and the Nagata RSF (right column), where Φ_0 and τ_0 are steady-state values for V_0.

Table 2
Simulation results ([]*: 10^3V_0 is chosen for V_c instead of 10^6V_0).

RSF#	t_{int}[year]	Δt_{pre}[year]	$\Delta\tau_{pre}$[MPa]	$\Delta\Phi_{pre}$[MPa]
N-0	−13	1.2	3.6	28
N-2	−67	2.0	4.9	76
N-4	−70	2.0	4.6	122
A-0	−29	1.5	4.3	51
A-2	−58	2.2	6.1	150
A-4	−64	2.2	5.9	245
B-0	−16	[0.73]*	[0.6]*	[17]*
B-2	−55	[0.83]*	[2.1]*	[60]*
B-4	−65	[0.89]*	[1.9]*	[95]*

the strength drop in its preslip period was further incresed to $\Delta\Phi_{pre}=$ 122 MPa. The simulation result with N-4 thus supports our interpretation from the inspection of the formula mentioned above.

5.2.2. Robustness of the tendencies

So far, we have successfully identified two distinct effects of Nagata RSF on earthquake cycles. One is an earlier strength reduction during the still firmly locked stage and the other is a larger strength drop in the preslip period. Our simulations shown so far were all based on a single experimental data set, that is, data N. Although data N are quantitatively typical among rock friction data at room temperature, some quantitative variations are known from laboratory even within similar conditions. Furthermore, hydrothermal environments for natural earthquakes can modify frictional properties to some significant extent (e.g., Blanpied et al., 1992; Nakatani and Scholz, 2004a). Although our focus is to elucidate the effects of the new 'formula', this would not exempt us from some basic checks of the robustness of the claimed characteristics over a range of likely quantitative variations of frictional properties. For this reason, we additionally examine seismic cycles based on two additional sets of supplementary data A and data B as described in Section 3.2; data A represent friction with larger a and the same $(b\text{-}a)$ as the data N, while data B represent friction with the same a and larger $(b\text{-}a)$. We conduct additional six simulations with frictional parameter sets of A-0, A-2, A-4, B-0, B-2 and B-4 in Table 1. We again assume the same loading velocity $V_0=4.5$ cm/year, the same stiffness $k=5.0$ MPa/m, 10^5 times larger L for L^{sim}. By adjusting v, recurrence interval in each simulation is set to $T_r=100$ years. Assumed parameters are listed in Table 1.

As to simulations with A-0, A-2 and A-4 summarized in Table 2, the two features of Nagata-RSF cycles discussed in the last subsection based on data N are supported. With an increasing degree of Nagataness, we see earlier start of the strength drop, starting at $t^{int}=-29,-58,-64$ years for A-0, A-2, A-4, respectively. The strength drop in the latter two cases clearly started within the well-locked interseismic stage, whereas the result with A-0 (pure Dieterich) showed that the strength started decreasing as slip-weakening became significant later in the cycle. The other feature of the much larger strength drop $\Delta\Phi_{pre}$ in the preslip period by the Nagata RSF is also preserved, with $\Delta\Phi_{pre}$ being 51, 150, 245 MPa for A-0, A-2, A-4, respectively. On the other hand, again, not much difference was seen in the stress drop $\Delta\tau_{pre}$ during the preslip period.

Data B represents a strong velocity-weakening friction and hence tend to lead to extremely unstable behaviors. In order to tame the cycles so that they have the recurrence interval of 100 years and the stress drop of 22.5 MPa the same as the others, simulations with B-0, B-2, and B-4 had to be done with very large v-values (Table 1). Such extremely large values of damping coefficient, however, overly suppressed slip velocity during dynamic instability, where the radiation damping term became important in Eq. (11). As a result, the peak seismic slip velocities in these simulations were of the order of 10^5V_0(~0.14 mm/s). Although the dynamic phase of the cycle was grossly miscalculated in these simulations, results for the quasi-static period should be basically intact. By examining the relative importance of the damping term in Eq. (11), we have found that the quasi-static phase ends when V exceeds about 10^3V_0. Hence, for these simulations with B-0, B-2, and B-4, we set $V_c=10^3V_0$ and measured quantities characterizing the preslip accordingly. That's why those values for B-0, B-2, and B-4 are asterisked in Table 2. Though asterisked, the results of B-series simulations support both claimed characteristics of the Nagata RSF. With an increasing degree of Nagataness, we see earlier start of the strength drop, starting at $t^{int}=-16,-55,-65$ years for B-0, B-2, B-4, respectively. Note that t^{int} is not affected by the definition of V_c. The strength reduction in the latter two cases clearly started within the well-locked interseismic stage, whereas the result with B-0 (pure Dieterich) showed that the strength started decreasing as slip-weakening became significant. The other feature of much larger strength drop $\Delta\Phi_{pre}$ in the preslip following the Nagata RSF is also preserved, with $\Delta\Phi_{pre}$ being 17, 60, 95 MPa for B-0, B-2, B-4, respectively. Also note that these $\Delta\Phi_{pre}$ values are generally smaller than those in the corresponding cases of N-series or A-series. This may be interpreted as a general tendency that more 'brittle' friction leads to less emphasized preslip. The preslip in B-series simulations is indeed the least remarkable also in terms of Δt_{pre} or $\Delta\tau_{pre}$.

Seeing the robustness shown above, we conclude that the two tendencies of the seismic cycles simulated with the Nagata RSF identified in Section 5.2.1 are significant differences made by the RSF revision.

6. Discussion: Strength drop as a detectable short-term precursor

Nagata et al. (2008, 2012) conducted rock friction experiments in a double-direct-shear apparatus, where they simultaneously measured P-wave transmissivity across the frictional interface to monitor the state of contact. The acoustic transmissivity $|T|$ was found to reflect changes in the contact state Φ very well (Fig. 1). All the present simulation results with the Nagata RSF showed a fairly large strength drop $\Delta\Phi_{pre}$ in the preslip period (Table 2), which is localized within a few years preceding the earthquake. This suggests a possibility of earthquake forecast by monitoring the strength drop of natural faults by acoustic methodology. However, a critical problem is that how the acoustic monitoring can be realized at a natural scale and its feasibility have to be discussed.

The acoustic method for monitoring mechanical properties of imperfectly welded interfaces was proposed by Kendall and Tabor (1971) and has been mainly studied in Engineering (e.g., Pyrak-Nolte et al., 1990). Such interfaces are supported by asperity contacts and characterized by the specific stiffness

$$\kappa = N\cdot cEr = N\kappa_0, \tag{12}$$

where N is the number of contacts per unit area, c is a constant around 2 depending on the Poisson's ratio, E is the Young modulus, r is the characteristic contact radius and $\kappa_0=cEr$ (unit; Pa/m) is the stiffness due to a single contact (Kendall and Tabor, 1971; Yoshioka and Iwase, 2006). Note that κ_0 is proportional to the radius r, not to the area πr^2. General solution for $|T|$ has been obtained for wave equation with this boundary as

$$|T| = \sqrt{\frac{1}{1+(\omega/\omega_c)^2}} \qquad (\omega_c = 2\kappa/Z) \tag{13}$$

where Z is acoustic impedance, ω is angular frequency, and $\omega_c=2\kappa/Z$ is a cutoff angular frequency for the low-pass ω-dependency of $|T|$; it decreases from about 1 to 0.1 with increase of ω from $0.1\omega_c$ to $10\omega_c$ (Kendall and Tabor, 1971; Schoenberg, 1980). $|T|$ is sensitive to κ in this frequency range.

Obviously monitoring acoustic transmissivity should be done in this range and the order of ω_c in the field is estimated below.

We start from the laboratory experiment of Nagata et al. (2008) of the order of $\Phi^{lab} \sim 10$ MPa, $f_c^{lab} (= \omega/2\pi) \sim 1$ MHz and $r^{lab} \sim L^{lab} \sim 1\mu$m, where r is considered to be comparable to the characteristic slip distance L (Yoshioka and Iwase, 1996). For the simulation values of $\Phi^{sim} = 10\Phi^{lab}$ and $r^{sim} = 10^5 r^{lab}$, f_c^{sim} can be estimated as follows: 1) Because Φ is proportional to real contact area A_r (Dieterich and Kilgore, 1996), $A_r^{sim} (= N^{sim}\pi(r^{sim})^2)$ is ten times greater than $A_r^{lab} (= N^{lab}\pi(r^{lab})^2)$, which gives $N^{sim} = N^{lab} \cdot 10/(10^5)^2$. 2) The specific stiffness is then given by Eq. (12) as $\kappa^{sim} = N^{sim} \cdot cEr^{sim} = 10/10^5 \kappa^{lab}$. 3) Finally $f_c^{sim} = 10/10^5 f_c^{lab} = 100$ Hz. More generally I times greater Φ^{sim} and J times greater r^{sim} lead to $f_c^{sim} = (I/J) f_c^{lab}$. Recently large $L \sim 1$ m (Hori and Miyazaki, 2011; Kato and Yoshida, 2011) and weak $\Phi =$ 10 MPa (Hasegawa et al., 2011) were reported for the 2012 Mw9.0 Tohoku earthquake. If we take these values, f_c could be as low as 1 Hz. We think that the frequency range between 1 to 100 Hz is seismically observable. In fact, the explosion reflection surveys conducted over the plate boundary on the forearc slope of the Japan Trench successfully revealed the intensity distribution of plate boundary *PP* reflection around 5 ~ 20 Hz (Fujie et al., 2002; Mochizuki et al., 2005). Because acoustic reflection $|R|$ is theoretically related to $|T|$ (Schoenberg, 1980), acoustic monitoring of Φ via $|R|$ looks feasible at the natural scale. Note that though expected change of $|T|$ in the preslip period would depend on the ratio of $\Delta\Phi_{pre}$ to absolute value of Φ (Nagata et al., 2012), the ratio is arbitrary in the simulations (only the change from an arbitrarily chosen reference value is necessary). The ratio could be more than 50% if a weak fault is considered in our simulation ($\Delta\Phi_{pre} = 76$ MPa in Table 2 and $\Delta\Phi$ in the whole cycle is about 150 MPa in Fig. 5), and it would be easily detected by seismic reflection surveys.

Short-term preslip is sometimes thought to be a key precursor of the impending earthquake and has been extensively examined in earthquake cycle simulations (e.g., Kato and Hirasawa, 1999; Kato and Tullis, 2003). However, the simulated preslip is usually so small that the resulting crustal deformation is hard to detect at geodetic stations on the Earth's surface far from the preslipping fault at depth. In contrast, acoustic methodology may enable us to monitor Φ remotely. One important point is that the acoustic transmissivity has a linear sensitivity on Φ (Nagata et al, 2008, 2012). Roughly saying, this means that the sensitivity is linear with respect to *logV*, not *V*. This is very advantageous to pick up changes by orders of magnitude but remaining in a very low absolute velocity range. Such is exactly the case in the preslip period in our simulation results. Although the strength drop in the preslip period results from the slip weakening by the small preslip displacement, either in the Nagata RSF or the Dieterich RSF, the acoustically monitorable change is fairly large, proportional to $\Delta\Phi$. While the expected amount of preslip is only a minuscule fraction of the coseismic slip, strength (i.e., Φ) drop in the same period is as large as several tens of percent of the strength change over the whole cycle. Furthermore, if the correct friction law for natural faults is the Nagata RSF as is the case for laboratory experiments, the strength drop and the accompanying change of acoustic transmissivity is even larger than previously calculated with the Dieterich RSF. Although Nagata et al. (2008) pointed out such possibilities of acoustic monitoring, their experiments were artificially imposed hold-slide cycles, not spontaneous stick-slip cycles, whereas the present numerical study has confirmed that the hope is still kept when put into the context of spontaneous stick-slip cycles under the slow tectonic loading at a constant rate.

7. Conclusion

On the basis of the revised RSF proposed by Nagata et al. (2012), we re-investigated the mechanics of frictional stick-slip cycles of earthquake faults.

Firstly, we analyzed the long-term stability of a spring-slider system. Analytic expression for the critical stiffness k_c has been derived and validated successfully. The RSF revision led to that faults are about 30 percent more stable than previously estimated from the original (Dieterich) RSF description of the same laboratory data.

Secondly, we compared regular stick-slip cycles simulated with the original (Dieterich) RSF and the revised (Nagata) RSF in order to identify major consequences of the revision. Our results showed significant differences in state evolution in both the interseismic and preslip periods. The state with the revised RSF turns to decrease as early as at one third of the recurrence interval, when the fault is still locked firmly at a negligible slip velocity. This is a straightforward manifestation of the newly introduced stress-weakening effect. On the other hand, in the preslip period where slip velocity is no more negligible compared to the load-point velocity, the Nagata RSF undergoes a three times larger reduction of the strength Φ. This results from the larger slip-weakening rate b/L, which has been increased by several times by the Nagata revision. Our simulation results suggest that monitoring of the state, instead of slip, would be more advantageous to detect the preslip phase of an earthquake cycle. Finally, robustness of all these conclusions has been confirmed by additional simulations over a range of parameter values.

Acknowledgments

Comments by A. Rubin and an anonymous reviewer are greatly appreciated. Discussion with K. Nagata was helpful. N. Kato provided his numerical code. N.K. was supported by MEXT Grant-in-Aid for Scientific Research on Innovative Areas Number 21107007. This study was also supported by MEXT, under its Observation and Research Program for Prediction of Earthquakes and Volcanic Eruptions.

References

Ampuero, J.P., Rubin, A.M., 2008. Earthquake nucleation on rate and state faults — Aging and slip laws. Journal of Geophysical Research 113 (B01302). http://dx.doi.org/10.1029/2007JB005082.

Beeler, N.M., Tullis, T.E., Weeks, J.D., 1994. The roles of time and displacement in the evolution effect in rock friction. Geophysical Research Letters 21, 1987–1990. http://dx.doi.org/10.1029/94GL01599.

Blanpied, M.L., Lockner, D.A., Byerlee, J.D., 1992. An earthquake mechanism based on rapid sealing of faults. Nature 358, 574–576. http://dx.doi.org/10.1038/358574a0.

Brechet, Y., Estrin, Y., 1994. The effect of strain rate sensitivity on dynamic friction of metals. Scripta Metallurgica et Materialia 30, 1449–1454.

Chambon, G., Schimittbuhl, J., Corfdir, A., Orellana, N., Diraison, M., Geraud, Y., 2006. The thickness of faults: from laboratory experiments to field scale observations. Tectonophysics 426, 77–94.

Dieterich, J.H., 1979. Modeling of rock friction 1. Experimental results and constitutive equations. Journal of Geophysical Research 84, 2161–2168.

Dieterich, J.H., 1992. Earthquake nucleation on faults with rate- and state-dependent strength. Tectonophysics 211, 115–134.

Dieterich, J.H., 1994. A constitutive law for rate of earthquake production and its application to earthquake clustering. Journal of Geophysical Research 99, 2601–2618.

Dieterich, J.H., Kilgore, B.D., 1996. Imaging surface contacts: power law contact distributions and contact stresses in quartz, calcite, glass and acrylic plastic. Tectonophysics 256, 219–239.

Fujie, G., Kasahara, J., Hino, R., Sato, T., Shinohara, M., Suehiro, K., 2002. A significant relation between seismic activities and reflection intensities in the Japan Trench region. Geophysical Research Letters 29. http://dx.doi.org/10.1029/2001GL013746.

Gu, J.C., Rice, J.R., Ruina, A.L., Tse, S.T., 1984. Slip motion and stability of a single degree of freedom elastic system with rate and state dependent friction. Journal of the Mechanics and Physics of Solids 32, 167–196.

Hasegawa, A., Yoshida, K., Okada, T., 2011. Nearly complete stress drop in the 2011 Mw 9.0 off the Pacific coast of Tohoku Earthquake. Earth, Planets and Space 63, 703–707.

Heslot, F., Baumberger, T., Perrin, B., Caroli, B., Caroli, C., 1994. Creep, stick-slip, and dry-friction dynamics: experiments and a heuristic model. Physical Review E 49, 4973–4988.

Hori, T., Miyazaki, S., 2011. A possible mechanism of M9 earthquake generation cycles in the area of repeating M7-8 earthquakes surrounded by aseismic sliding. Earth, Planets and Space 63, 773–777.

Kame, N., Fujita, S., Nakatani, M., Kusakabe, T., 2012. Effects of a revised rate- and state-dependent friction law on aftershock triggering model. Tectonophysics 600, 187–195.

Kato, N., Hirasawa, T., 1999. A model for possible crustal deformation prior to a coming large interplate earthquake in the Tokai district, central Japan. Bulletin of the Seismological Society of America 89, 1401–1417.

Kato, N., Tullis, T.E., 2001. A composite rate- and state-dependent law for rock friction. Geophysical Research Letters 28, 1103–1106. http://dx.doi.org/10.1029/2000GL012060.

Kato, N., Tullis, T.E., 2003. Numerical simulation of seismic cycles with a composite rate- and state-dependent friction law. Bulletin of the Seismological Society of America 93, 841–853.
Kato, N., Yoshida, S., 2011. A shallow strong patch model for the 2011 great Tohoku-oki earthquake: a numerical simulation. Geophysical Research Letters 38 (L00G04). http://dx.doi.org/10.1029/2011GL048565.
Kendall, K., Tabor, D., 1971. An ultrasonic study of the area of contact between stationary and sliding surfaces. Proceedings of the Royal Society of London, Series A 323, 321–340.
Lapusta, N., Rice, J.R., Ben-Zion, Y., Zheng, G., 2000. Elastodynamic analysis for slow tectonic loading with spontaneous rupture episodes on faults with rate- and state-dependent friction. Journal of Geophysical Research 105 (B10), 23765–23789. http://dx.doi.org/10.1029/2000JB900250.
Marone, C., 1995. Fault zone strength and failure criteria. Geophysical Research Letters 22, 723–726. http://dx.doi.org/10.1029/95GL00268.
Marone, C., Kilgore, B., 1993. Scaling of the critical slip distance for seismic faulting with shear strain in fault zones. Nature 362, 618–621.
Marone, C., Scholz, C.H., Bilham, H., 1991. On the mechanics of earthquake afterslip. Journal of Geophysical Research 96 (B5). http://dx.doi.org/10.1029/91JB00275.
Mochizuki, K., Nakamura, M., Kasahara, J., Hino, R., Nishino, M., Kuwano, A., Nakamura, Y., Yamada, T., Shinohara, M., Sato, T., Moghadham, P.P., Kanazawa, T., 2005. Intense *PP* reflection beneath the aseismic forearc slope of the Japan Trench subduction zone and its implication of aseismic slip subduction. Journal of Geophysical Research 110 (B01302). http://dx.doi.org/10.1029/2003JB002892.
Nagata, K., Nakatani, M., Yoshida, S., 2008. Monitoring frictional strength with acoustic wave transmission. Geophysical Research Letters 35. http://dx.doi.org/10.1029/2007GL033146.
Nagata, K., Nakatani, M., Yoshida, S., 2012. A revised rate- and state-dependent friction law obtained by constraining constitutive and evolution laws separately with laboratory data. Journal of Geophysical Research 117 (B2). http://dx.doi.org/10.1029/2011JB008818.
Nakatani, M., 2001. Conceptual and physical clarification of rate and state friction: frictional sliding as a thermally activated rheology. Journal of Geophysical Research 106 (B7), 13347–13380. http://dx.doi.org/10.1029/2000JB900453.
Nakatani, M., Mochizuki, H., 1996. Effects of shear stress applied to surfaces in stationary contact on rock friction. Geophysical Research Letters 23, 869–872. http://dx.doi.org/10.1029/96GL00726.
Nakatani, M., Scholz, C.H., 2004a. Frictional healing of quartz gouge under hydrothermal conditions: 1. Experimental evidence for solution transfer healing mechanism. Journal of Geophysical Research 109 (B07201). http://dx.doi.org/10.1029/2001JB001522.
Nakatani, M., Scholz, C.H., 2004b. Frictional healing of quartz gouge under hydrothermal conditions: 2. Quantitative interpretation with a physical model. Journal of Geophysical Research 109 (B07202). http://dx.doi.org/10.1029/2003JB002938.
Press, W.H., Teukolsky, S.A., Vetterling, W.T., Flannery, B.P., 1992. Numerical Recipes, 2nd. ed. Cambridge Univ. Press, New York.
Pyrak-Nolte, L.J., Myer, L.R., Cook, N.G., 1990. Transmission of seismic waves across single natural fractures. Journal of Geophysical Research 95, 8617–8638. http://dx.doi.org/10.1029/JB095iB06p08617.
Rice, J.R., 1993. Spatio-temporal complexity of slip on a fault. Journal of Geophysical Research 98, 9885–9907.
Rice, J.R., Ben-Zion, Y., 1996. Slip complexity in earthquake fault models. Proceedings of the National Academy of Sciences of the United States of America 93, 3811–3818.
Rice, J.R., Lapusta, N., Ranjith, K., 2001. Rate and state dependent friction and the stability of sliding between elastically deformable solids. Journal of the Mechanics and Physics of Solids 49, 1865–1898.
Rubin, A.M., Ampuero, J.P., 2005. Earthquake nucleation on (aging) rate and state faults. Journal of Geophysical Research 110 (B11312). http://dx.doi.org/10.1029/2005JB003686.
Ruina, A., 1983. Slip instability and state variable friction laws. Journal of Geophysical Research 88, 10359–10370.
Schoenberg, M., 1980. Elastic wave behavior across linear slip interfaces. Journal of the Acoustical Society of America 68, 1516–1521.
Scholz, C.H., Engelder, J.T., 1976. The role of asperity indentation and ploughing in rock friction -I. Asperity creep and stick slip. International Journal of Rock Mechanics and Mining Science and Geomechanics 13, 149–154.
Weeks, J., 1993. Constitutive laws for high-velocity frictional sliding and their influence on stress drop during unstable slip. Journal of Geophysical Research 98, 17, 637–17, 648.
Yoshioka, N., Iwase, K., 1996. The characteristic displacement in rate and state-dependent friction from a micromechanical point of view. Pure and Applied Geophysics 147, 433–453.
Yoshioka, N., Iwase, K., 2006. A laboratory experiment to monitor the contact state of a fault by transmission waves. Tectonophysics 413, 221–238.